

Research Article

Shahid Khan, Mahmoud M. Selim*, Khaled A. Gepreel, Asad Ullah, Ikramullah, Muhammad Ayaz, Wali Khan Mashwani, and Emel Khan

An analytical investigation of the mixed convective Casson fluid flow past a yawed cylinder with heat transfer analysis

<https://doi.org/10.1515/phys-2021-0040>

received November 20, 2020; accepted April 24, 2021

Abstract: The hydrodynamic flow of an incompressible and isotropic Casson fluid through a yawed cylinder is investigated by employing continuity, momentum, and energy equations satisfying suitable boundary conditions. The density variation is governed by Boussinesq approximation. The model equations consisting of coupled partial differential equations (PDEs) are transformed by applying non-similar transformation relations. The set of transformed PDEs is solved using the analytical technique of homotopy analysis method (HAM). The impacts of varying yaw angle, and mixed convection and Casson parameters over fluid velocity (chordwise and spanwise components), its temperature, Nusselt number, and skin

friction coefficients are investigated and explained through various graphs. It is found that the enhancing yaw angle, Casson parameter, and convection parameter augment the fluid velocity, heat transfer rate, and skin friction and reduce the fluid temperature. The agreement of present and published results justifies the application of HAM in modeling the mixed convective Casson fluid flow past a yawed cylinder.

Keywords: Casson fluid, yawed cylinder, mixed convection, thermal radiations, PDEs, HAM

1 Introduction

The fluid flow past yawed and unyawed objects extensively occurs in various engineering-related applications, like cables suspensions bridge, chimney stacks, different towers, sub-sea pipelines, risers, heat exchangers, and overhead cables. Sears [1] was the first who studied boundary layer fluid flow along yawed cylinder by considering different cylinders in yawed condition. Then, Chiu and Lienhard [2] investigated the flow past a cylinder in yawed condition and found the point of separation independent of yaw angle. The analyse of complex flow patterns around yawed cylindrical cables, mitigation of the drag forces, and the suppression of modulation in lift forces are the important phenomena encountered in the engineering manufacturing design. The researchers have performed experimental [3–5] and numerical [6] investigations of the fluid flowing past a yawed cylinder. The experimental findings showed that the normalized force coefficients are almost independent of yaw angle. This result is termed as cosine law or independence principle. It is relatively simple to investigate the laminar fluid flow over yawed cylinder by assuming constant fluid characteristics. In practical situations, there exists temperature difference between ambient fluid and cylinder surface, due to which different fluid properties, such as Prandtl

* **Corresponding author: Mahmoud M. Selim**, Department of Mathematics, Al-Aflaj College of Science and Humanities Studies, Prince Sattam bin Abdulaziz University, Al-Aflaj 710-11912, Saudi Arabia; Department of Mathematics, Suez Faculty of Science, Suez University, Suez 34891, Egypt, e-mail: m.selim@psau.edu.sa
Shahid Khan: Department of Mathematics, Institute of Numerical Sciences, Kohat University of Science & Technology, Kohat 26000, Khyber Pakhtunkhwa, Pakistan, e-mail: shahidkhan@kust.edu.pk
Wali Khan Mashwani: Department of Mathematics, Institute of Numerical Sciences, Kohat University of Science & Technology, Kohat 26000, Khyber Pakhtunkhwa, Pakistan, e-mail: mashwanigr8@gmail.com
Emel Khan: Department of Mathematics, Institute of Numerical Sciences, Kohat University of Science & Technology, Kohat 26000, Khyber Pakhtunkhwa, Pakistan, e-mail: emelkhan.ek@gmail.com
Khaled A. Gepreel: Department of Mathematic, Faculty of Science, Taif University, P.O. Box 11099, Taif 21944, Saudi Arabia, e-mail: k.gepreel@tu.edu.sa
Asad Ullah: Department of Mathematical Sciences, University of Lakki Marwat, K.P., 28420, Pakistan, e-mail: asad@ulm.edu.pk
Ikramullah: Department of Physics, Kohat University of Science & Technology, Kohat 26000, Khyber Pakhtunkhwa, Pakistan, e-mail: ikramullah@kust.edu.pk
Muhammad Ayaz: Department of Mathematics, Abdul Wali Khan University, Mardan 23200, Khyber Pakhtunkhwa, Pakistan, e-mail: mayazmath@awkum.edu.pk

number, density, viscosity, etc., vary with space and time, which influence the temperature and velocity fields during the fluid motion. In situations where moderate or high temperature gradient exists, the assumption of constant fluid properties may produce quite large errors in computing the different macroscopic properties of the fluid flow. The recent investigations about boundary layer laminar flow with varying fluid properties are performed in refs. [2,7–8]. In current years, the non-similar solutions to the non-steady fluid flow have gained importance in fluid mechanics as well as in mass and heat energy transfer phenomena. The solution of steady flow through the non-similarity solution method is presented by Deway and Gross [9]. Roy [10] as well as Roy and Saikrishnan [11] obtained non-similar solutions for the steady laminar boundary layer motion past yawed cylinder possessing varying physical aspects for compressible and non-compressible fluids, respectively. The study of Dufour and Soret effects over the motion of magnetized Jeffery nanofluid motion toward an extendable cylinder is carried out by Jagan *et al.* [13] considering the combined impacts of triple stratification, radiation, and slip. The governing equations are transformed to ordinary differential equations (ODEs) through similarity transformations, and solved through homotopy analysis method (HAM). The variation in concentration and temperature profiles is studied using the Dufour and Soret numbers' varying values. The time variation in the non-steady fluid flow complicates the process of obtaining the non-similar solutions. The investigations of solving non-steady boundary layer flow problems using the non-similar solutions technique are smaller in number in comparison with the investigations through similarity [12] and semi-similar [7] solutions techniques. Eswara and Nath [13] investigated the non-steady, laminar, and incompressible flow in stagnation region of axisymmetric and 2D bodies in the magnetic field (**B**-field) presence. During their investigation, they observed that skin friction depends strongly, whereas the heat energy transport depends weakly, on the strength of the magnetic parameter. Furthermore, heat energy transfer and the skin friction are found to depend strongly on the mass transfer parameter. Roy *et al.* [14] examined the non-steady mixed convection fluid flow over a vertical conical surface through non-similar solution. Some of the excellent reviews about the non-steady fluid flow can be consulted in refs. [15–18]. Thumma *et al.* [19] examined the 3D migration of Casson fluid taking into account the impacts of Lorentz force, zigzag motion of minute particles, thermal radiation, chemical reaction, heat source presence, etc. The modeled ODEs governing the MHD Casson fluid are solved using the hybrid collection numerical

scheme based on Newton–Raphson iterative scheme (NRIS) and generalized differential quadrature method (GDQM) and briefly investigated are the impacts of associated physical variables over the Casson fluid motion. Rehman *et al.* [20] undertook the flow characteristics of magnetized Eyring–Powell fluid migration induced by a stretching cylindrical surface considering the impacts of Joule heating and mixed convection. Ashraf *et al.* [21] used GDQM to model and investigate the MHD peristaltic nanofluid flow. A number of research studies on the mixed convective flow topic have been undertaken from almost last 60 years. The researchers have contributed outstanding results to the scientific literature by analyzing the mixed convective fluid flow using various geometries. Wakif [22] employed novel numerical procedure to simulate magnetized Casson fluid convective flow over an irregular geometrical horizontal extendable sheet by considering the impacts of thermal conductivity and viscosity (temperature dependent). Surprisingly, the mixed convective fluid migration past a cylinder in yawed condition has not been so far investigated sufficiently. Bückner and Lueptow [23] in 1998 analyzed experimentally the turbulent flow of the boundary layer past a yawed condition cylinder. The research works in refs. [24–26] have explored the different aspects of forced convective motion near yawed cylinder. Ponnaiah [25] and Revathi *et al.* [26] studied the slot mass transfer problem past cylinder in yawed configuration. Roy and Saikrishnan [11] investigated the water boundary layer motion along yawed cylinder. Recently, Patil *et al.* [27] analyzed the mixed convective thermal energy transfer flow across a yawed cylinder. The study is modeled by appropriate equations and then solved through the quasi-linearization [28–30] and finite difference techniques [31,32]. The authors found that the fluid speed, frictional forces, and heat energy transfer rate augment, while the fluid temperature drops due to mixed convective flow. Furthermore, the yaw angle has significant contribution in enhancing the chordwise and spanwise fluid velocities for increasing mixed convection variable.

In the current work, the laminar and incompressible Casson fluid through a yawed cylinder is analytically investigated by employing continuity, momentum, and energy equations. HAM is applied for the solution of governing equations. The novelty of the current study is the analytical investigation of the Casson fluid motion past a yawed cylinder. The structure of the article goes as follows: the geometry and mathematical modeling of the study are given in Section 2. The HAM technique used to solve the set of governing equations is elaborated in Section 3. The results are discussed through displayed plots in Section 4. The comparison of the

$$\left(1 + \frac{1}{\gamma}\right) S_{\eta\eta} + \frac{1}{3}(f + 2\xi f_\xi) S_\eta - \frac{2}{3} \xi F S_\xi + \lambda_i I(\xi) \Theta \sin(\theta) = 0, \quad (9)$$

$$\Theta_{\eta\eta} + \frac{\text{Pr}}{3}(f + 2\xi f_\xi) \Theta_\eta - \frac{2}{3} \xi \text{Pr} F \Theta_\xi = 0, \quad (10)$$

$$\begin{aligned} F = 0, \quad S = 0, \quad \Theta = 1, \quad \text{at } \eta = 0 \\ F \rightarrow 1, \quad S \rightarrow 1, \quad \Theta \rightarrow 0, \quad \text{at } \eta \rightarrow \infty. \end{aligned} \quad (11)$$

Here, $\text{Pr} = \frac{\rho C_p \nu}{k}$ is the Prandtl number, f and ψ are non-dimensional and dimensional stream functions, respectively, $\lambda_i = \frac{g \beta_T (T_w - T_\infty) R}{\tilde{U}_e^2}$ is the mixed convection variable,

F and S are the chordwise and spanwise dimensionless velocities, respectively. Furthermore, Θ is the dimensionless temperature, and the quantities $\Omega(\xi)$, $l(\xi)$, and $I(\xi)$ are defined as follows:

$$\Omega(\xi) = \frac{2\xi}{\tilde{U}_e} \frac{d\tilde{U}_e}{d\xi}, \quad l(\xi) = \frac{\xi}{4 \cos^3 \bar{x}}, \quad I(\xi) = \frac{\xi}{2 \cos^2 \bar{x}}.$$

The transformed velocity components are given as follows:

$$\begin{aligned} u &= \tilde{U}_e F(\xi, \eta), \\ v &= -\frac{\tilde{U}_\infty}{3} \left(\frac{2\nu\xi}{\tilde{U}_\infty} \right)^{0.5} \left(\frac{f}{\xi} \cos(\bar{x}) + 2f_\xi \cos(\bar{x}) \right. \\ &\quad \left. - 3\eta F \tan(\bar{x}) - \frac{\eta}{\xi} \cos(\bar{x}) F \right), \\ w &= W_e S(\xi, \eta). \end{aligned} \quad (12)$$

The relation between ξ and \bar{x} can be established with the following transformation:

$$\xi \frac{\partial}{\partial \xi} = \varepsilon(\bar{x}) \frac{\partial}{\partial \bar{x}}, \quad (13)$$

where $\varepsilon(\bar{x}) = \tan \bar{x}$.

Now, $\xi(\bar{x})$, $\Omega(\bar{x})$, $l(\bar{x})$, and $I(\bar{x})$ as functions of \bar{x} are given by the following equations.

$$\begin{aligned} \xi(\bar{x}) &= \frac{2}{3} \sin \bar{x}, \quad \Omega(\bar{x}) = -\tan^2 \bar{x}, \\ l(\bar{x}) &= \frac{\sin \bar{x}}{6 \cos^3 \bar{x}} \quad \text{and} \quad I(\bar{x}) = \frac{\sin \bar{x}}{3 \cos^2 \bar{x}}. \end{aligned} \quad (14)$$

Using equations (13) and (14) in equations (8)–(11), we get:

$$\begin{aligned} \left(1 + \frac{1}{\gamma}\right) F_{\eta\eta} + \frac{1}{3}(2\varepsilon(\bar{x})f_{\bar{x}} + f) F_\eta + \frac{\Omega(\bar{x})}{3}(1 - f^2) \\ - \frac{2}{3} \varepsilon(\bar{x}) F F_{\bar{x}} + \lambda_i l(\bar{x}) \Theta \sin(\theta) = 0, \end{aligned} \quad (15)$$

$$\begin{aligned} \left(1 + \frac{1}{\gamma}\right) S_{\eta\eta} + \frac{1}{3}(2\varepsilon(\bar{x})f_{\bar{x}} + f) S_\eta - \frac{2}{3} \varepsilon(\bar{x}) F S_{\bar{x}} \\ + \lambda_i I(\bar{x}) \Theta \sin(\theta) = 0, \end{aligned} \quad (16)$$

$$\Theta_{\eta\eta} + \frac{\text{Pr}}{3}(2\varepsilon(\bar{x})f_{\bar{x}} + f) \Theta_\eta - \frac{2}{3} \varepsilon(\bar{x}) \text{Pr} F \Theta_{\bar{x}} = 0. \quad (17)$$

The boundary constraints are as follows:

$$\begin{aligned} F(\bar{x}, 0) = 0, \quad S(\bar{x}, 0) = 0, \quad \Theta(\bar{x}, 0) = 1, \\ \text{at } \eta = 0, \\ F(\bar{x}, 0) \rightarrow 1, \quad S(\bar{x}, 0) \rightarrow 1, \quad \Theta(\bar{x}, 0) \rightarrow 0, \\ \text{as } \eta \rightarrow \infty. \end{aligned} \quad (18)$$

The relations for chordwise and spanwise skin frictions, and the Nusselt number are, respectively, given as follows:

$$\text{Re}^{0.5} C_f = 4\sqrt{3} \left(1 + \frac{1}{\gamma}\right) \frac{\cos^2 \bar{x}}{\sqrt{\sin \bar{x}}} F_\eta(\bar{x}, 0), \quad (19)$$

$$\text{Re}^{0.5} C_f^* = 2\sqrt{3} \left(1 + \frac{1}{\gamma}\right) \cot(\theta) \frac{\cos \bar{x}}{\sqrt{\sin \bar{x}}} S_\eta(\bar{x}, 0), \quad (20)$$

$$\text{Re}^{-0.5} \text{Nu} = -\sqrt{3} \frac{\cos \bar{x}}{\sqrt{\sin \bar{x}}} \Theta_\eta(\bar{x}, 0). \quad (21)$$

3 Solution by HAM

In engineering sciences, majority of the problems are nonlinear in nature and are difficult to solve with the existing numerical methods. Since 1992, after the work of Liao [36], analytical methods are widely used to handle such complex problems. The HAM can solve both nonlinear ODEs and partial differential equations (PDEs). If the similarity solution exists, then the original problem reduces to the nonlinear ODEs. Solution of such problems can be seen in refs. [37–39]. On the other hand, if the similarity solution does not exist, then the original problem can not reduce to ODEs. Thus, the transformed problem retains its PDEs nature. Such problems are not widely seen in the literature. The reason behind this rareness is the solution of coupled non-linear PDEs, which is always a tough task for the researchers [40]. The mechanism for such complex problems is explained by Liao in “Homotopy Analysis Method in non-linear differential equations” [41]. In this method, the transformed problem retains its PDEs nature. The basic mechanism of HAM depends on the following functional relation:

$$\tilde{\Psi} : \hat{X} \times [0, 1] \rightarrow \hat{Y}. \quad (22)$$

Here, $\tilde{\Psi}[\hat{x}, 0] = \zeta_1(\hat{x})$ and $\tilde{\Psi}[\hat{x}, 1] = \zeta_2(\hat{x})$ hold $\forall \hat{x} \in \hat{X}$, while, $\zeta_1(\hat{x})$ and $\zeta_2(\hat{x})$ are the elements of \hat{X} and \hat{Y} spaces. The set of equations (15)–(18) are solved through HAM by

choosing the non-linear operators $N_F(\bar{F})$, $N_S(\bar{S})$, and $N_\Theta(\bar{\Theta})$ with the corresponding initial guesses F_0 , S_0 , and Θ_0 .

4 Results and discussion

Here, we explain the variation of various aspects of Casson fluid flow with varying yaw angle θ , Casson fluid, and mixed convection parameters (γ, λ_i) by depicting plots for chordwise (F) and spanwise (S) velocity components, dimensionless temperature, skin friction coefficients, and Nusselt number.

Figure 2(a and b) depicts the dependence of the velocity $F(\eta)$ (chordwise direction) on varying θ (yaw angle) at different mixed convection parameter λ_i values. Figure 2(a) is plotted for $\lambda_i = -2$, whereas Figure 2(b) is plotted for $\lambda_i = 10$. The values of θ used are $\theta = 15^\circ, 30^\circ, 45^\circ, 60^\circ$.

Figure 2(a) shows that the velocity displays a descending behavior with the rising θ . Figure 2(b) displays that the velocity in the chordwise direction shows an augmenting trend with the rising θ . The enhancement in the chordwise fluid velocity ($F(\eta)$) with the rising θ due to aiding buoyancy flow ($\lambda_i = 10$) is due to the more tilting of the cylinder, which develops a pressure gradient and causes the fluid to move faster. Whereas in the case of opposing buoyancy flow ($\lambda_i = -2$), the velocity in the chordwise direction drops with the enhancing yaw angle θ .

Figure 3 displays the dependence of $F(\eta)$ on varying Casson parameter (γ) and mixed convection parameter λ_i values. Figure 3(a) is plotted for $\lambda_i = -2$, whereas Figure 3(b) is plotted for $\lambda_i = 10$. The different values of γ used in displaying Figure 3 are $\gamma = 2, 4, 6, 8$. It is clear from Figure 3(a) that the chordwise velocity reduces with the augmenting values of λ_i . Figure 3(b) displays that adding buoyancy ($\lambda_i = 10$) results in an enhancement in

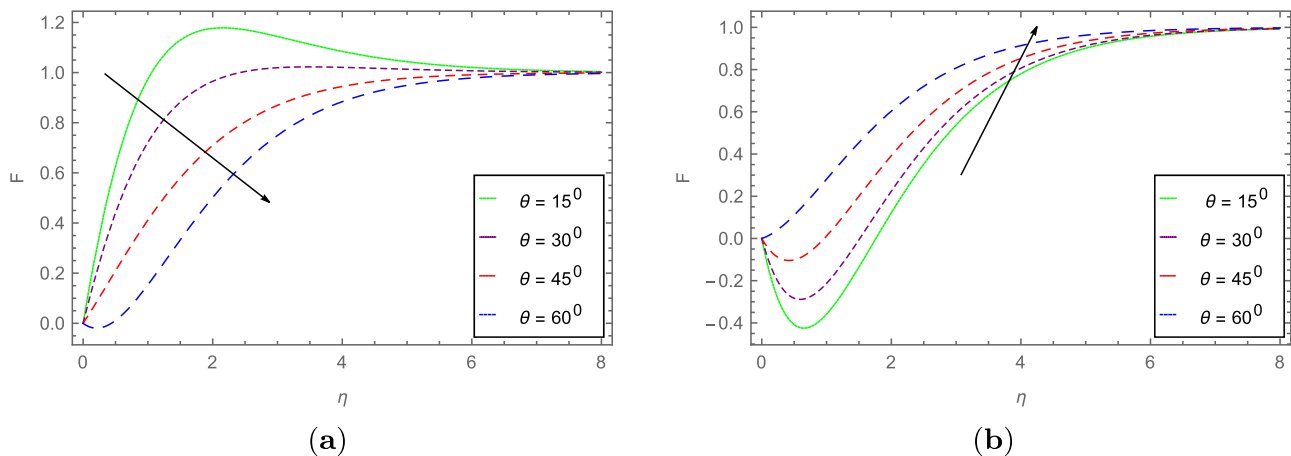


Figure 2: Influence of θ on (a) $F(\eta)$ for $\lambda_i = -2$ and (b) $F(\eta)$ for $\lambda_i = 10$.

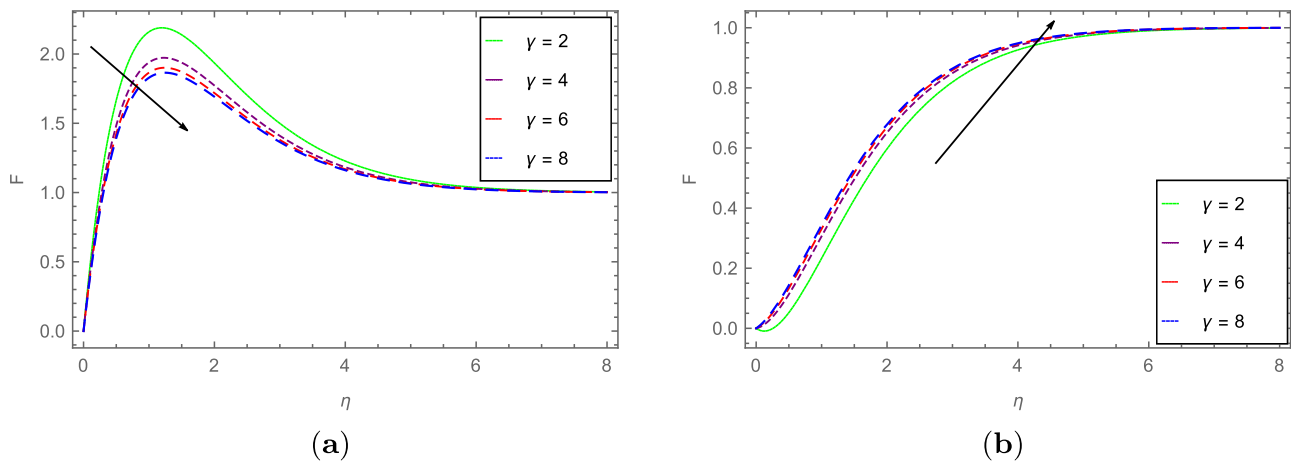


Figure 3: Impact of γ on (a) $F(\eta)$ for $\lambda_i = -2$ and (b) $F(\eta)$ for $\lambda_i = 10$.

the chordwise fluid velocity of the Casson fluid. Therefore, it can be concluded that aiding buoyancy to the Casson fluid flow enhances the spanwise velocity with the rising Casson fluid parameter (higher γ means approaching toward Newtonian fluid character).

The behavior of the spanwise velocity component ($S(\eta)$) with the changing θ (yaw angle) and mixed convection parameter λ_i is depicted in Figure 4. Figure 4(a) is depicted for $\lambda_i = -2$, while Figure 4(b) is plotted for $\lambda_i = 10$, respectively. It is apparent from Figure 4(a) that the spanwise velocity augments with the opposing buoyancy. From Figure 4(b) we see that spanwise velocity S profiles drop with the enhancing values of θ . Thus, the chordwise velocity drops with the increasing yaw angle due to aiding buoyancy flow. This means that in case of aiding buoyancy flow, the chordwise velocity component drops with the augmenting values of the yaw angle,

whereas the opposing buoyancy flow shows an opposite impact on the chordwise velocity component.

The effects of changing Casson parameter (γ) and the mixed convection parameter λ_i on $S(\eta)$ (the spanwise velocity component) are depicted in Figure 5. Figure 5(a) is depicted for $\lambda_i = -2$, whereas Figure 5(b) is plotted for $\lambda_i = 10$, respectively. The first graph shows that $S(\eta)$ varies directly with the rising η at fixed γ . The $S(\eta)$ profiles shift to higher values with the augmenting γ up to $\eta = 6.0$ and then overlap with one another. The dependence of $S(\eta)$ on the varying γ for $\lambda_i = 10$ is displayed in Figure 5(b). The behavior of $S(\eta)$ in this case with the augmenting θ looks to be completely opposite to that of Figure 5(a). It is therefore concluded that aiding buoyancy to the Casson fluid flow depreciates the spanwise fluid velocity, while augments it in case of opposing buoyancy with increasing Casson fluid parameter (γ) values.

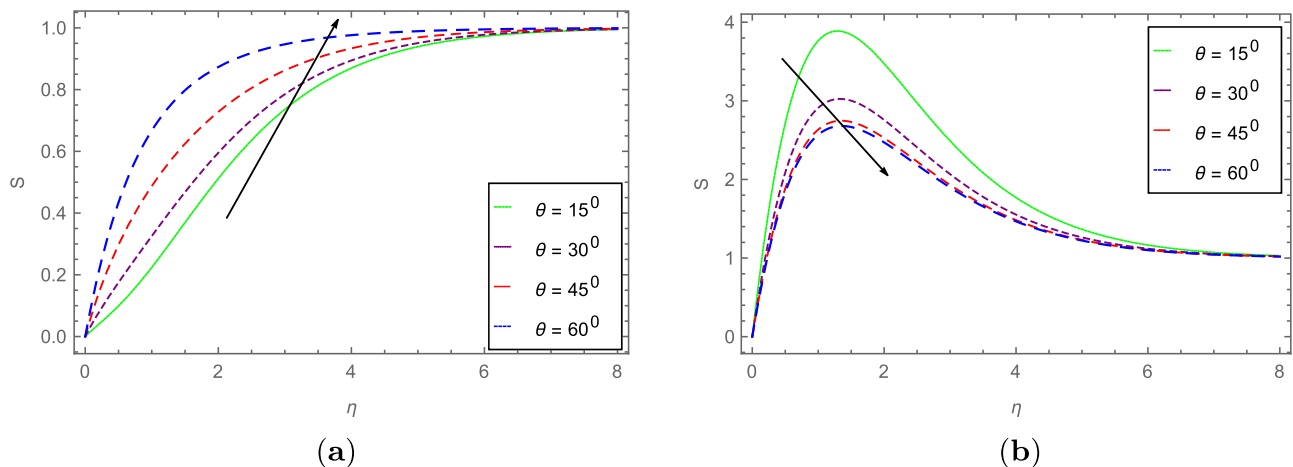


Figure 4: Impact of θ on (a) $S(\eta)$ for $\lambda_i = -2$ and (b) $S(\eta)$ for $\lambda_i = 10$.

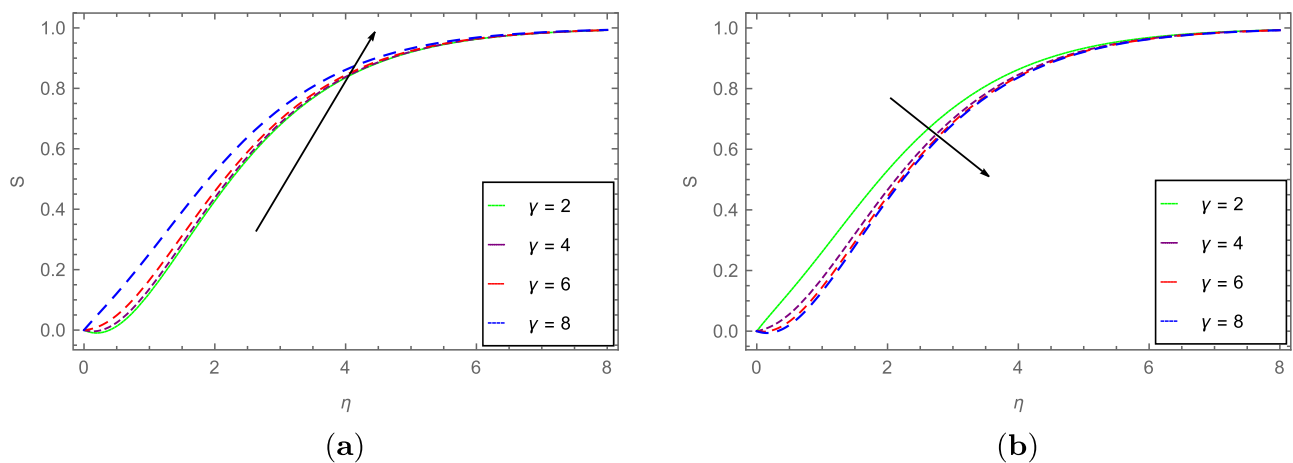


Figure 5: Impact of γ on (a) $S(\eta)$, for $\lambda_i = -2$ and (b) $S(\eta)$ for $\lambda_i = 10$.

The variation of the dimensionless temperature ($\Theta(\eta)$) with the changing values of θ and mixed convection parameter λ_i is shown in Figure 6. Figure 6(a) is plotted for $\lambda_i = -2$, while Figure 6(b) is depicted for $\lambda_i = 10$, respectively. The values of θ used are $\theta = 15^\circ, 30^\circ, 45^\circ, 60^\circ$. Figure 6(a) shows that with increasing θ , the $\Theta(\eta)$ profiles shift to higher values. Figure 6(b) displays the functional dependence of $\Theta(\eta)$ on η with changing θ for the higher value of the mixed convection parameter λ_i . We see that the fluid temperature $\Theta(\eta)$ reduces with the augmenting values of the yaw angle. The reducing behavior of the fluid temperature for the rising θ with aiding buoyancy flow (larger λ_i) is due to the enhancing fluid velocity, which carries away more heat from the cylinder surface and thus causing the Casson fluid temperature to drop.

The variations of the skin friction in the chordwise direction with changing yaw angle θ and mixed convection

parameter λ_i are shown in Figure 7. Figure 7(a) is plotted for $\lambda_i = -2$ and $Pr = 7.0$, whereas Figure 7(b) is drawn for $\lambda_i = 10$ and $Pr = 7.0$, respectively. It is clear that the skin friction in the chordwise direction enhances with the increasing yaw angle at higher value of mixed convection parameter λ_i . This enhancement in the skin friction is due to the higher Casson fluid velocity with the augmenting yaw angle at higher λ_i (aiding buoyancy flow) as observed in Figure 2(b).

The impact of varying yaw angle θ and mixed convection flow parameter λ_i on the spanwise skin friction is shown in Figure 8. Figure 8(a) is plotted for $\lambda_i = -2$ and $Pr = 7.0$, whereas Figure 8(b) is drawn for $\lambda_i = 10$ and $Pr = 7.0$, respectively. From these figures, it is clear that the spanwise skin friction drops with the augmenting values of yaw angle for both opposing and aiding buoyancy flows. The skin friction drops with the aiding buoyancy as shown in Figure 8(b), which is due to the slip

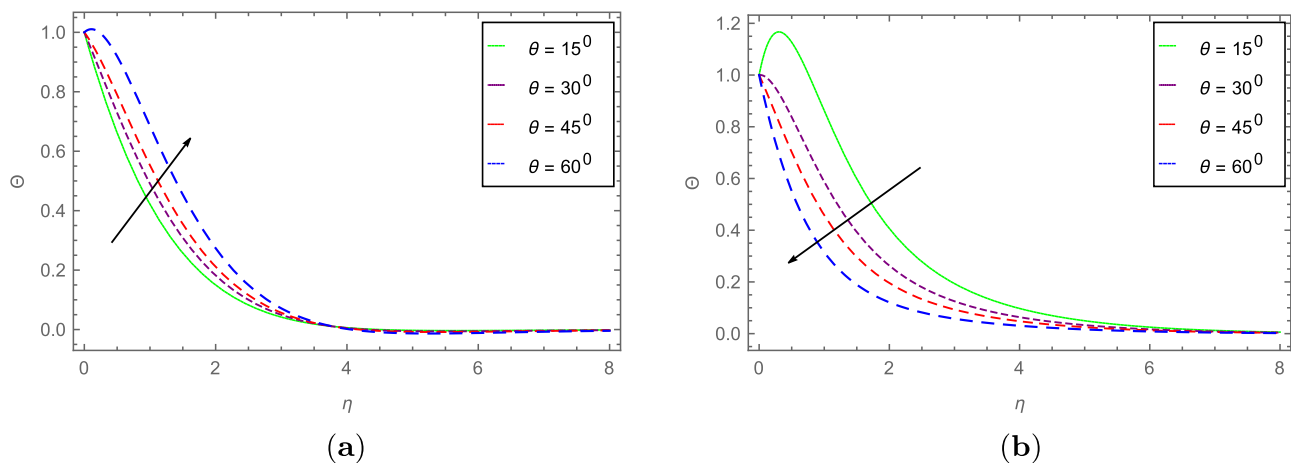


Figure 6: Impact of θ on (a) $\Theta(\eta)$, for $\lambda_i = -2$ and (b) $\Theta(\eta)$ for $\lambda_i = 10$.

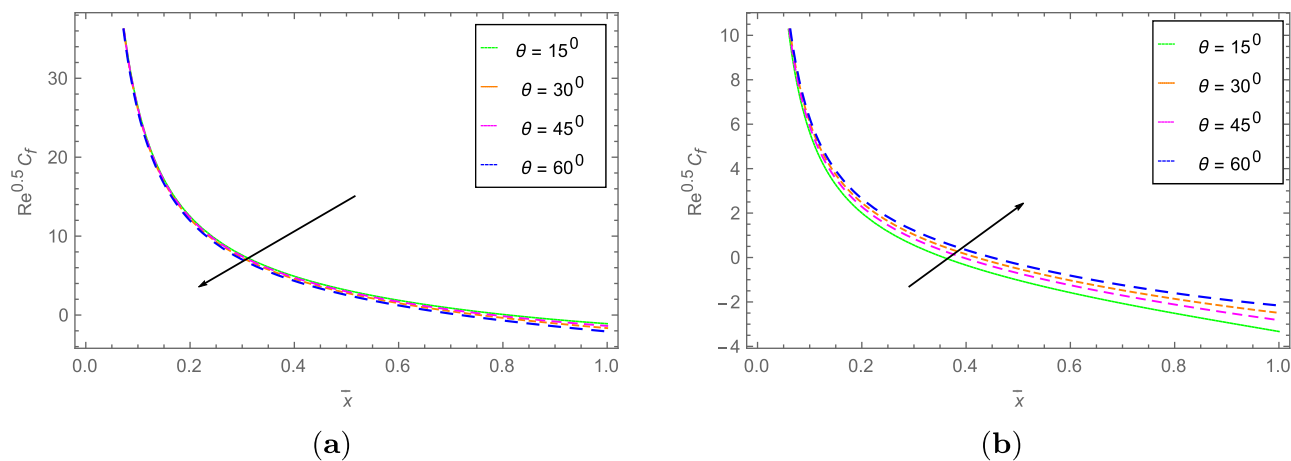


Figure 7: Dependence of chordwise skin friction for (a) $\lambda_i = -2$ and (b) $\lambda_i = 10$ with varying θ at $Pr = 7.0$.

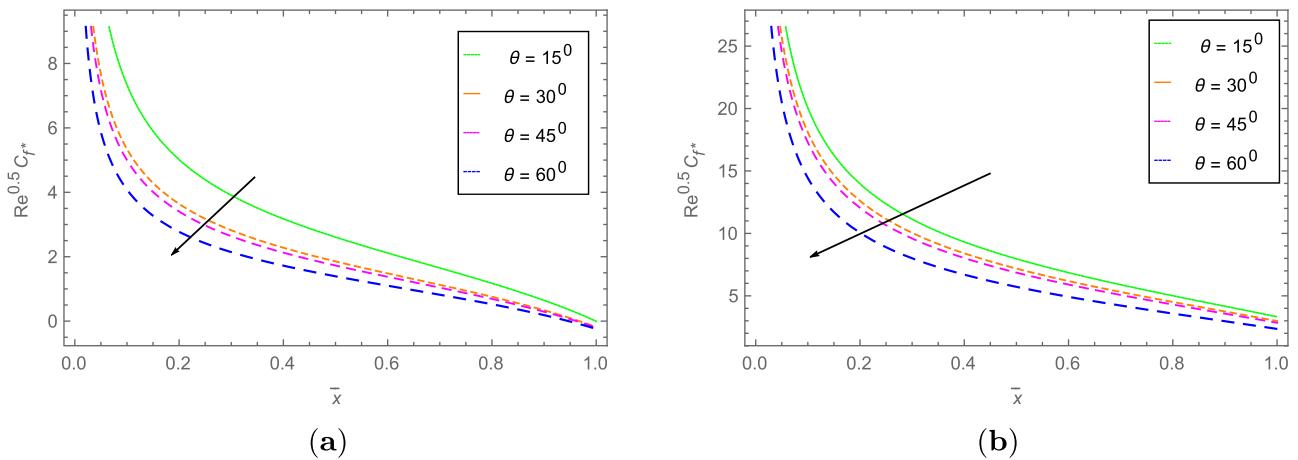


Figure 8: Dependence of spanwise skin friction for (a) $\lambda_i = -2$ and (b) $\lambda_i = 10$ with the varying yaw angle at $Pr = 7.0$.

experienced by the Casson fluid in the spanwise direction, although the spanwise velocity augments with the aiding buoyancy flow as given in Figure 4(a).

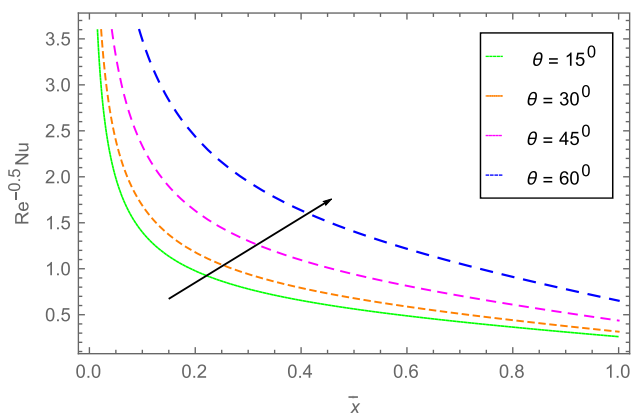


Figure 9: Heat transfer enhancement when $\lambda_i = 10$ and $Pr = 7.0$.

Figure 9 depicts the variation of the Nusselt number with changing values of the yaw angle θ for the aiding buoyancy flow ($\lambda_i = 10$). It is clear that the thermal energy transfer flow augments with the rising yaw angle. This enhancement in the thermal energy transfer with the rising yaw angle is due to the augmenting Casson fluid flow velocity, which carries away more heat from the cylinder surface, and causing the Nusselt number to augment.

The dependence of chordwise velocity F and spanwise velocity S on the non-similarity variable \bar{x} is depicted in Figure 10. The values of the other parameters are taken as $\lambda_i = 10$ and $Pr = 7.0$. It is apparent from the figures, that both velocities enhance with augmenting \bar{x} , that is moving away from the origin of the coordinate system. The higher value of \bar{x} corresponds to the more tilting configuration of the yawed cylinder, which causes to enhance the Casson fluid velocities in both chordwise and spanwise directions.

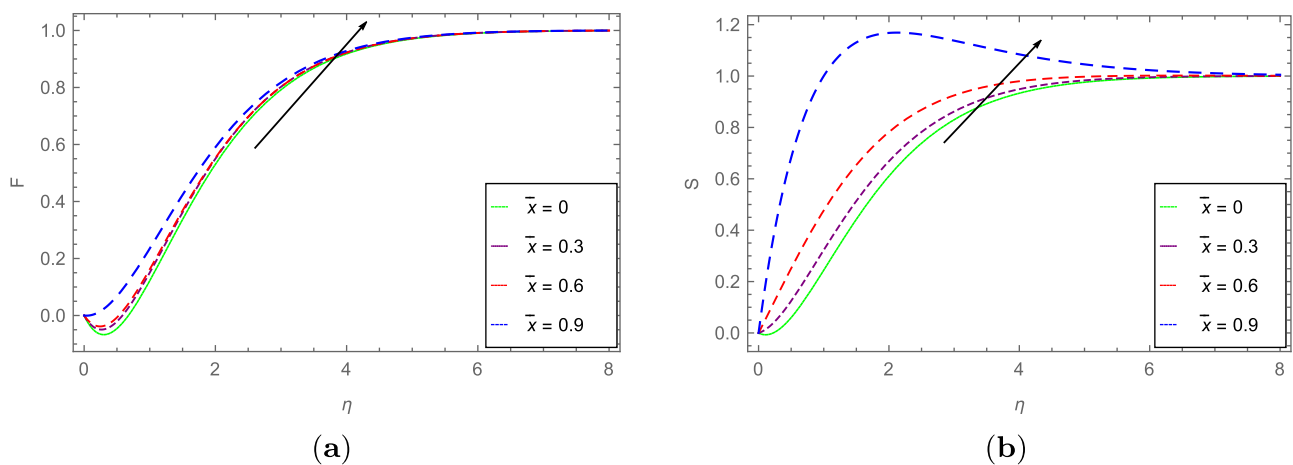


Figure 10: Dependence of (a) chordwise velocity and (b) spanwise velocity on \bar{x} for $\lambda_i = 10$ and $Pr = 7.0$.

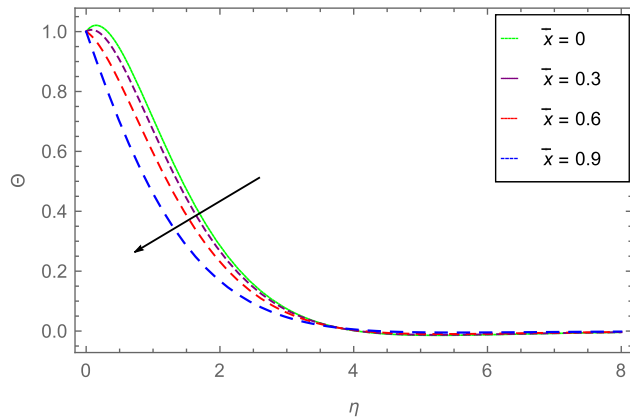


Figure 11: Temperature variation with \bar{x} , when $\lambda_i = 10$ and $Pr = 7.0$.

The variation of the dimensionless temperature (Θ) with varying \bar{x} is displayed in Figure 11. The values of the other parameters are taken as $\lambda_i = 10$ and $Pr = 7.0$. It is observed that the temperature drops as one moves away from the origin (with rising \bar{x}). The drop in the temperature with the augmenting \bar{x} is due to the enhancing fluid velocities (F , S) as observed in Figure 10.

5 Validation of HAM

The comparison of the results achieved in this study with the results obtained in ref. [27] is displayed in Table 1. In Table 1, the skin friction (spanwise direction) and Nusselt number are computed with changing values of \bar{x} and λ_i . The first and second columns show the variation in \bar{x} and λ_i , respectively. The third and fourth columns represent the numerical values of skin friction and Nusselt number obtained in ref. [27]. The last two columns show the results of skin friction and Nusselt number computed

Table 1: Variations in skin friction and Nusselt number for $\theta = 0^\circ$ and $Pr = 0.7$

\bar{x}	λ_i	$Re^{0.5} C_{f^*}$ ref. [28]	$Re^{-0.5} Nu$ ref. [28]	Present ($Re^{0.5} C_{f^*}$)	Present ($Re^{-0.5} Nu$)
0	0	1.3282	0.5853	1.32823	0.58532
0	1	4.9664	0.8220	4.96641	0.82204
0	2	7.7120	0.9304	7.71201	0.93043
1	0	1.9169	0.8667	1.91694	0.86672
1	1	5.2578	1.0618	5.25782	1.06183
1	2	7.8864	1.1686	7.88644	1.16862
2	0	2.3974	1.0965	2.39742	1.09653
2	1	5.6995	1.2713	5.69952	1.27133
2	2	8.3556	1.3743	8.35561	1.37433

in the current investigation. Table 1 shows the accuracy of our currently employed technique HAM (analytical), which is in a complete agreement with the previously used technique (numerical).

6 Conclusions

The outcomes of the current investigations are outlined in this section. The hydrodynamic flow of an incompressible and isotropic Casson fluid through a yawed cylinder is analytically examined. The governing equations are simplified by using non-similar transformation relations. The standard analytical procedure of HAM is used to solve the developed system of equations. The influence of varying strength of yaw angle, mixed convection, and Casson fluid parameters over the velocity components (chordwise and spanwise), dimensionless temperature, skin friction coefficients, and heat transfer rate are investigated and explained with the help of different graphs. During this study, the following results are concluded:

- The enhancing yaw angle and Casson parameter augment the chordwise velocity $F(\eta)$ at higher mixed convection parameter λ_i (aiding buoyancy flow), while opposite variation is observed for smaller λ_i (opposing buoyancy flow).
- The spanwise velocity $S(\eta)$ enhances with the rising yaw angle and Casson parameter for opposing buoyancy flow, while drops with aiding buoyancy flow.
- The Casson fluid temperature drops with the enhancing yaw angle with aiding buoyancy flow.
- The chordwise skin friction augments, while the spanwise skin friction drops with the rising yaw angle at higher λ_i .
- The increasing yaw angle enhances the heat energy transfer rate.
- The comparison of the obtained and published results shows an outstanding agreement that justifies the accuracy of the applied technique.

Abbreviations

The below mentioned parameters and abbreviations with their possible dimensions are used in this article.

β_T	expansion of thermal coefficient $\frac{1}{K}$
μ_b	dynamic plastic viscosity $\frac{kg}{ms}$
μ_b	dynamic plastic viscosity $\frac{kg}{ms}$

T	fluid temperature K
μ_b	dynamic plastic viscosity $\frac{\text{kg}}{\text{ms}}$
γ	Casson fluid parameter $\frac{\text{kg}}{\text{ms}}$
α	thermal conductivity $\frac{\text{W}}{\text{mK}}$
C_p	specific heat $\left(\frac{\text{J}}{\text{kg K}}\right)$
∞	condition at infinity
0	reference condition
$x, y, \text{ and } z$	coordinates (m)
Pr	Prandtl number
λ_i	mixed convective parameter
Θ	dimensionless temperature
C_f	skin friction
Re	local Reynolds number
F	chordwise dimensionless velocity
S	spanwise dimensionless velocity
Ψ	stream function
ρ	density $\left(\frac{\text{kg}}{\text{m}^3}\right)$
t	time (s)
\tilde{U}_∞	constant velocity along x -direction $\left(\frac{\text{m}}{\text{s}}\right)$
\tilde{W}_∞	constant velocity along z -direction $\left(\frac{\text{m}}{\text{s}}\right)$
\tilde{x}	dimensionless distance along the surface
W_e	velocity at the edge of the boundary layer $\left(\frac{\text{m}}{\text{s}}\right)$
U_e	potential flow velocity at the edge of the boundary layer $\left(\frac{\text{m}}{\text{s}}\right)$
η, ζ	transformed coordinates
θ	yawed angle (Degree)

Acknowledgments: The research was supported by the Taif University Researchers Supporting Project number (TURSP-2020/16), Taif University, Taif, Saudi Arabia.

Funding information: The authors received financial support from the Taif University Researchers Supporting Project Number (TURSP-2020/16), Taif University, Taif, Saudi Arabia.

Conflict of interest: The authors declare no conflict of interest.

References

- [1] Sears WR. The boundary layer of yawed cylinders. *J Aeronaut Sci.* 1948;15(1):49–52.
- [2] Chiu W, Lienhard J. On real fluid flow over yawed circular cylinders. *J Basic Eng.* 1967;89(4):851–7.
- [3] King R. Vortex excited oscillations of yawed circular cylinders. *J Fluids Eng.* 1977;99:495–502.
- [4] Ramberg S. The effects of yaw and finite length upon the vortex wakes of stationary and vibrating circular cylinders. *J Fluid Mechanics.* 1983;128:81–107.
- [5] Thakur A, Liu X, Marshall J. Wake flow of single and multiple yawed cylinders. *J Fluids Eng.* 2004;126(5):861–70.
- [6] Marshall J. Wake dynamics of a yawed cylinder. *J Fluids Eng.* 2003;125(1):97–103.
- [7] Vasantha R, Nath G. Semi-similar solution of an unsteady compressible three-dimensional stagnation point boundary layer flow with massive blowing, *Int J Eng Sci.* 1985;23(5):561–69.
- [8] Cooke J. The boundary layer of a class of infinite yawed cylinders. In: *Mathematical proceedings of the Cambridge philosophical society.* vol. 46. no. 4. Cambridge: Cambridge University Press; 1950. p. 645–8.
- [9] Dewey Jr. CF, Gross JF. Exact similar solutions of the laminar boundary-layer equations. In: *Advances in heat transfer.* vol. 4. Cambridge: Elsevier; 1967. p. 317–446.
- [10] Roy S. Non-uniform mass transfer or wall enthalpy into a compressible flow over yawed cylinder. *Int J Heat Mass Transfer.* 2001;44(16):3017–24.
- [11] Roy S, Saikrishnan P. Non-uniform slot injection (suction) into water boundary layer flow past yawed cylinder. *Int J Eng Sci.* 2004;42(19–20):2147–57.
- [12] Jagan K, Sivasankaran S, Bhuvaneswari M, Rajan S, Makinde OD. Soret and Dufour effect on MHD Jeffrey nanofluid flow towards a stretching cylinder with triple stratification, radiation and slip. In: *Defect and diffusion forum*, vol. 387. Switzerland: Trans Tech Publ; 2018. p. 523–33.
- [13] Eswara A, Nath G. Unsteady nonsimilar two-dimensional and axisymmetric water boundary layers with variable viscosity and Prandtl number. *Int J Eng Sci.* 1994;32(2):267–79.
- [14] Roy S, Datta P, Mahanti N. Non-similar solution of an unsteady mixed convection flow over a vertical cone with suction or injection. *Int J Heat Mass Transfer.* 2007;50(1–2):181–7.
- [15] Riley N. Unsteady laminar boundary layers. *SIAM review.* 1975;17(2):274–97.
- [16] McCroskey WJ. Current research in unsteady fluid dynamics-the 1976 freeman scholar lecture, trans. asme. *J Fluid Eng.* 1977;1:8–39.
- [17] Telionis D. Unsteady boundary layers, separated and attached. *J Fluids Eng.* 1979;101(1):29–43.
- [18] Telionis DP. *Unsteady viscous flows.* New York: Springer; 1981. vol. 9.
- [19] Thumma T, Wakif A, Animasaun IL. Generalized differential quadrature analysis of unsteady three-dimensional mhd radiating dissipative Casson fluid conveying tiny particles. *Heat Transfer.* 2020;49(5):2595–626.
- [20] Rehman K, Malik M, Makinde O. Parabolic curve fitting study subject to joule heating in MHD thermally stratified mixed convection stagnation point flow of Eyring-Powell fluid induced by an inclined cylindrical surface. *J King Saud Univ Sci.* 2018;30(4):440–9.
- [21] Ashraf MU, Qasim M, Wakif A, Afridi MI, Animasaun IL. A generalized differential quadrature algorithm for simulating magnetohydrodynamic peristaltic flow of blood-based nanofluid containing magnetite nanoparticles: A physiological application. *Numer Meth Partial Diff Equ.* 2020;1–27.
- [22] Wakif A. A novel numerical procedure for simulating steady mhd convective flows of radiative Casson fluids over a

- horizontal stretching sheet with irregular geometry under the combined influence of temperature-dependent viscosity and thermal conductivity. *Math Problems Eng.* 2020;2020:1–20.
- [23] Bückner D, Lueptow RM. The boundary layer on a slightly yawed cylinder. *Exp Fluids.* 1998;25(5–6):487–90.
- [24] Subhashini S, Takhar HS, Nath G. Non-uniform multiple slot injection (suction) or wall enthalpy into a compressible flow over a yawed circular cylinder. *Int J Thermal Sci.* 2003;42(8):749–57.
- [25] Ponnaiah S. Boundary layer flow over a yawed cylinder with variable viscosity. *Int J Numer Meth Heat Fluid Flow.* 2012;22(3):342–56.
- [26] Revathi G, Saikrishnan P, Chamkha A. Non-similar solutions for unsteady flow over a yawed cylinder with non-uniform mass transfer through a slot. *Ain Shams Eng J.* 2014;5(4):1199–206.
- [27] Patil P, Shashikant A, Roy S, Hiremath P. Mixed convection flow past a yawed cylinder. *Int Commun Heat Mass Transfer.* 2020;114:104582.
- [28] Patil P, Roy M, Roy S, Momoniat E. Triple diffusive mixed convection along a vertically moving surface. *Int J Heat Mass Transfer.* 2018;117:287–95.
- [29] Patil P, Shashikant A, Roy S, Momoniat E. Unsteady mixed convection over an exponentially decreasing external flow velocity. *Int J Heat Mass Transfer.* 2017;111:643–50.
- [30] Patil P, Ramane H, Roy S, Hindasageri V, Momoniat E. Influence of mixed convection in an exponentially decreasing external flow velocity. *Int J Heat Mass Transfer.* 2017;104:392–9.
- [31] Patil P, Shashikant A, Hiremath P. Diffusion of liquid hydrogen and oxygen in nonlinear mixed convection nanofluid flow over vertical cone. *Int J Hydrogen Energy.* 2019;44(31):17061–71.
- [32] Patil P, Pop I, Roy S. Unsteady heat and mass transfer over a vertical stretching sheet in a parallel free stream with variable wall temperature and concentration. *Numer Methods Partial Diff Equ.* 2012;28(3):926–41.
- [33] Walawender WP, Chen TY, Cala DF. An approximate Casson fluid model for tube flow of blood. *Biorheology.* 1975;12(2):111–9.
- [34] Chaturani P, Palanisamy V. Casson fluid model for pulsatile flow of blood under periodic body acceleration. *Biorheology.* 1990;27(5):619–30.
- [35] Bali R, Awasthi U. A Casson fluid model for multiple stenosed artery in the presence of magnetic field. *Appl Math.* 2012;3:436–441.
- [36] Liao S-J. The proposed homotopy analysis technique for the solution of nonlinear problems. Ph.D. dissertation, Ph.D. Thesis, Shanghai Jiao Tong University Shanghai; 1992.
- [37] Schlichting H, Gersten K. Boundary-layer theory, (2000). *Int J Aerospace Eng Hindawi.* 2000;2018;29–49. www.hindawi.com
- [38] Shah Z, Alzahrani EO, Dawar A, Ullah A, Khan I. Influence of Cattaneo-Christov model on Darcy-Forchheimer flow of micropolar ferrofluid over a stretching/shrinking sheet. *Int Commun Heat Mass Transfer.* 2020;110:104385.
- [39] Shah Z, Ullah A, Bonyah E, Ayaz M, Islam S, Khan I. Hall effect on titania nanofluids thin film flow and radiative thermal behavior with different base fluids on an inclined rotating surface. *AIP Advances.* 2019;9(5):055113.
- [40] Crane LJ. Flow past a stretching plate. *Zeitschrift für angewandte Mathematik und Physik ZAMP.* 1970;21(4):645–7.
- [41] Liao S. Homotopy analysis method in nonlinear differential equations. Germany: Springer; 2012.